

FINCH: Fresnel Incoherent Correlation Hologram

Joseph Rosen¹, Barak Katz¹ and Gary Brooker²

¹*Ben-Gurion University of the Negev*

Department of Electrical and Computer Engineering

P. O. Box 653, Beer-Sheva 84105

²*Johns Hopkins University*

Department of Biomedical Engineering and Microscopy Center,

Montgomery County Campus

9605 Medical Center Drive Suite 240, Rockville, MD 20850

¹*Israel*

²*USA*

1. Introduction

Holographic imaging offers a reliable and fast method to capture the complete three-dimensional (3D) information of the scene from a single perspective. However, holography is not widely applied to the regime of white-light imaging, because white-light is incoherent and in general creating holograms requires a coherent interferometer system. In this chapter we describe our recently invented method of acquiring incoherent digital holograms. The term incoherent digital hologram means that incoherent light beams reflected or emitted from real existing objects interfere with each other. The resulting interferogram is recorded by a digital camera and digitally processed to yield a hologram. This hologram is reconstructed in the computer so that 3D images appear on the computer's screen. The coherent optical recording is not applicable for the incoherent optics because interference between reference and object incoherent beams cannot occur. Therefore, different holographic acquisition methods should be employed for generating an incoherent digital hologram.

The oldest methods of recording incoherent holograms have made use of the property that every incoherent object is composed of many source points, each of which is self-spatial coherent and therefore can create an interference pattern with light coming from the point's mirrored image. Under this general principle, there are various types of holograms, including Fourier (Stroke & Restrick, 1965; Breckinridge, 1974) and Fresnel holograms (Lohmann, 1965; Cochran, 1966; Peters, 1966; Marathay, 1987; Mugnier et al., 1993). The process of beam interfering demands high levels of light intensity, extreme stability of the optical setup, and relatively narrow bandwidth light source. These limitations have prevented holograms from becoming widely used for many practical applications. More recently, three groups of researchers have proposed computing holograms of 3D incoherently illuminated objects from a set of images taken from different points of view

(Li et al., 2001; Sando et al., 2003; Shaked & Rosen, 2008; Park et al., 2009). This method, although it shows promising prospects, is relatively slow since it is based on capturing tens of scene images from different view angles. Another method is called scanning holography (Poon & Korpel, 1979; Schilling et al., 1997; Poon, 2004; Rosen et al., 2006; Poon, 2007) in which a pattern of Fresnel zone plates (FZPs) scans the object such that at each and every scanning position, the light intensity is integrated by a point detector. The overall process yields a Fresnel hologram obtained as a correlation between the object and FZP patterns.

Our recently proposed incoherent digital hologram is dubbed Fresnel incoherent correlation hologram (FINCH) (Rosen & Brooker, 2007a). The FINCH is actually based on a single channel on-axis incoherent interferometer. Like any Fresnel holography, in the FINCH the object is correlated with quadratic phase functions, but the correlation is carried out without any movement and without multiplexing the image of the scene. This chapter reviews the latest developments of the FINCH in the field of color holography, microscopy and imaging with a synthetic aperture.

Generally, in the FINCH system, light is reflected, or emitted, from a 3D object, propagates through a spatial light modulator (SLM), and is recorded by a digital camera. The SLM is used as a beam-splitter of the single-channel incoherent interferometer, such that each spherical beam originated from each object point is split into two spherical beams with two different curve radiuses. Incoherent sum of the entire interferences between all the couples of spherical beams creates the Fresnel hologram of the observed 3D object. When this hologram is reconstructed in the computer, the 3D properties of the object are revealed.

In the following sections we describe various aspects of the FINCH, including FINCH of reflected white light (Rosen & Brooker, 2007a), FINCH of fluorescence objects (Rosen & Brooker, 2007b), a FINCH-based holographic fluorescence microscope (Rosen & Brooker, 2008), and finally a hologram recorder in a mode of a synthetic aperture (Katz & Rosen, 2010).

2. General properties of Fresnel holograms

The type of hologram discussed in this review is the digital Fresnel hologram, which means that a hologram of a single point has the form of the well-known FZP. The axial location of the object point is encoded by the Fresnel number of the FZP, which is the technical term for the quantity of the rings density in the FZP. To understand the operation principle of any general Fresnel hologram, let us look on the difference between regular and Fresnel-holographic imaging systems. In classical imaging, image formation of objects at different distances from the lens results in a sharp image at the image plane for objects at only one position from the lens, as shown in Fig. 1(a). The other objects at different distances from the lens are out of focus. Fresnel holographic system, on the other hand, as depicted in Fig. 1(b), projects a set of rings known as the FZP onto the plane of the image for each and every point at every plane of the object being viewed. The depth of the points is encoded by the density of the rings such that points which are closer to the system project denser rings than distant points. Because of this encoding method, the 3D information in the volume being imaged is recorded into the recording medium. Therefore, each plane in the image space reconstructed from a Fresnel hologram is in focus at a different axial distance. The encoding is accomplished by the presence of one of the holographic systems in the image path. Each holographic system, coherent or incoherent, has a different method to project the FZP on the image plane. At this point it should be noted that this graphical description of projecting

FZPs by every object's point actually expresses the mathematical two dimensional (2D) correlation (or convolution) between the object function and the FZP. In other words, the methods of creating Fresnel holograms are different from each other by the way they spatially correlate the FZP with the 3D scene. Another issue to note is that the correlation should be done with a FZP that is somehow 'sensitive' to the axial locations of the object points. Otherwise, these locations are not encoded into the hologram. The systems described in this review satisfies the condition that the FZP is dependent on the axial distance of each and every object point. This means that indeed points, which are far from the system, project FZP with fewer cycles per radial length than nearby points, and by this condition the holograms can actually image the 3D scene properly.

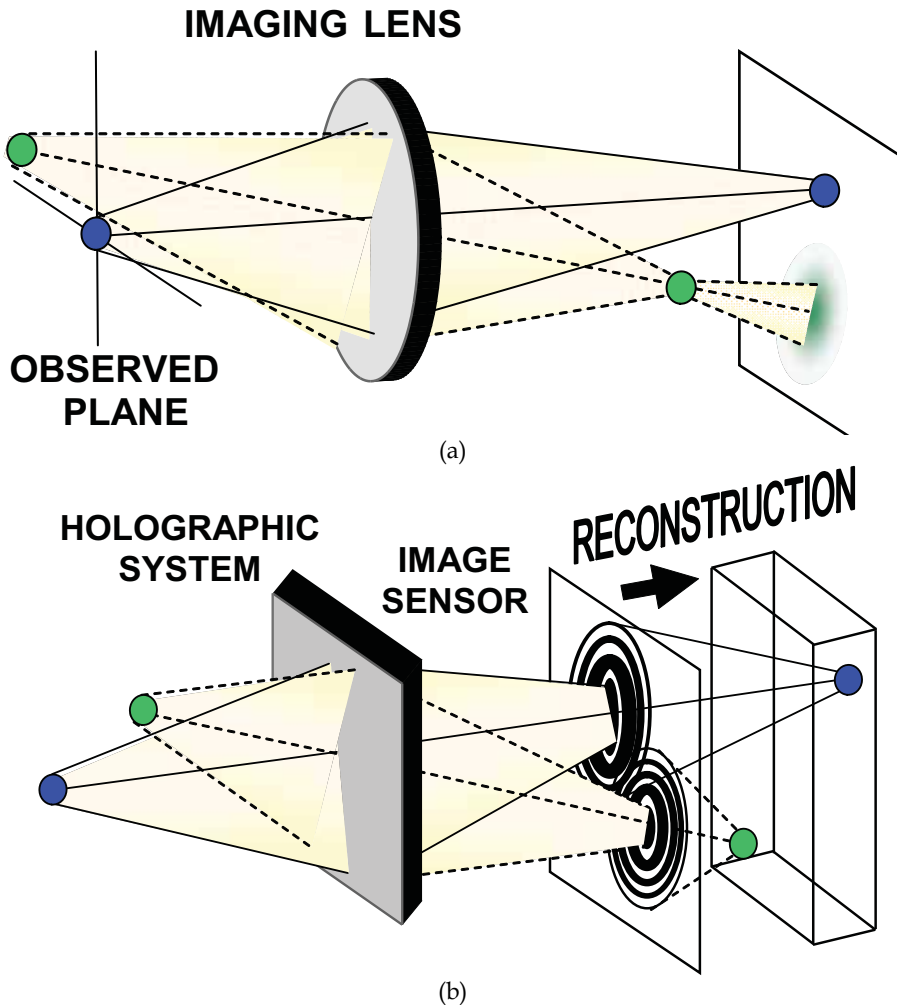


Fig. 1. Comparison of the Fresnel holography principle and conventional imaging. (a) Conventional imaging system. (b) Fresnel holography system.

The FZP is a sum of at least three main functions, a constant bias, a quadratic phase function and its complex conjugate. The object function is actually correlated with all these three functions. However the useful information, with which the holographic imaging is realized, is the correlation with just one of the two quadratic phase functions. The correlation with the other quadratic phase function induces the well-known twin image. This means that the detected signal in the holographic system contains three superposed correlation functions, whereas only one of them is the required correlation between the object and the quadratic phase function. Therefore, the digital processing of the detected signal should contain the ability to eliminate the two unnecessary terms.

The definition of Fresnel hologram is any hologram that contains at least, a correlation (or convolution) between an object function and a quadratic phase function. Moreover, the quadratic phase function must be parameterized according to the axial distance of the object points from the detection plane. In other words, the number of cycles per radial distance of each quadratic phase function in the correlation is dependent on the z distance of each object point. Formally, a hologram is called Fresnel hologram if its distribution function contains the following term:

$$H(u,v) = \iiint g(x,y,z) \exp\left\{i \frac{2\pi\beta}{z} \left[(u-x)^2 + (v-y)^2 \right]\right\} dx dy dz, \quad (1)$$

where $g(x,y,z)$ is the 3D object function and β is a constant. Indeed, in Eq. (1) the phase of the exponent is dependent on z , the axial location of the object. In case the object is illuminated by coherent wave, $H(u,v)$ given by Eq. (1) is the complex amplitude of the coherent electromagnetic field directly obtained, under the paraxial approximation (Goodman, 1996), by a free space propagation from the object to the detection plane. However, we deal here with incoherent illumination, for which alternative methods to the free propagation should be applied. In fact, in this chapter we describe such method to get the desired correlation with the quadratic phase function given in Eq. (1), and this method indeed operates under incoherent illumination. Like any Fresnel holography, in the FINCH the object is correlated with a FZP, but the correlation is carried out without any movement and without multiplexing the image of the scene. Section 3 reviews the latest developments of the FINCH in the field of holography, microscopy and incoherent synthetic aperture imaging.

3. Fresnel incoherent correlation holography

Various aspects of the FINCH have been described in the literature, including FINCH for reflected white light (Rosen & Brooker, 2007a), FINCH of fluorescence objects (Rosen & Brooker, 2007b), FINCHSCOPE (Rosen & Brooker, 2008) - a holographic fluorescence microscope and finally SAFE (Katz & Rosen, 2010) - a FINCH based process of recording incoherent holograms in a synthetic aperture mode.

Generally, in the FINCH system the reflected incoherent light from a 3D object propagates through a spatial light modulator (SLM) and is recorded by a digital camera. To solve the twin image problem, three holograms are recorded sequentially, each with a different phase factor of the SLM pattern. The three holograms are superposed in the computer such that the result is a complex-valued Fresnel hologram. The 3D properties of the object are revealed by reconstructing this hologram in the computer.

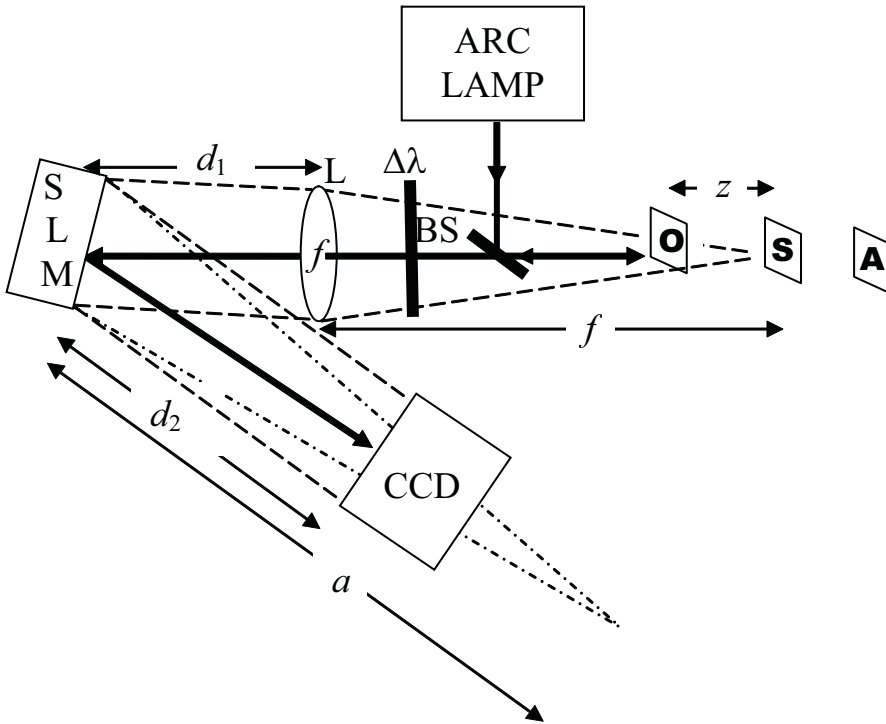


Fig. 2. Schematic of FINCH recorder. BS: beam splitter; SLM: spatial light modulator; CCD: charge-coupled device; L is a spherical lens with $f=25\text{cm}$ focal length. $\Delta\lambda$ indicates a chromatic filter with a bandwidth of $\Delta\lambda=60\text{nm}$.

3.1 FINCH for reflected white light

The first FINCH system (Rosen & Brooker, 2007a) is shown in Fig. 2. A white-light source illuminates a 3D object, and the reflected light from the object is captured by a digital camera after passing through a lens L and a SLM. In general, such a system can be analyzed as an incoherent correlator, where the SLM function is considered as a part of the system's transfer function. However, we find it easier to regard the system as an incoherent interferometer, where the grating displayed on the SLM is considered as a beam splitter. As is common in such cases, we analyze the system by following its response to an input object of a single infinitesimal point. Knowing the system's point spread function (PSF) enables one to realize the system operation for any general object. Analysis of a beam originated from a narrowband infinitesimal point source is done using Fresnel diffraction theory, (Goodman, 1996) since such a source is spatially coherent by definition.

A Fresnel hologram of a point object is obtained when the two interfering beams are, for instance, plane and spherical beams. Such a goal is achieved if the SLM's reflection function $R(x,y)$ is of the form

$$R(x,y) = \frac{1}{2} + \frac{1}{2} \exp \left[-\frac{i\pi}{\lambda a} (x^2 + y^2) + i\theta \right] = \frac{1}{2} + \frac{1}{2} Q \left(-\frac{1}{a} \right) \exp(i\theta). \quad (2)$$

For the sake of shortening, the quadratic phase function is designated by the function Q , such that $Q(b)=\exp[(i\pi b/\lambda)(x^2+y^2)]$. When a plane wave hits the SLM, the first constant term $1/2$ in Eq. (2) represents the reflected plane wave, and the quadratic phase term is responsible for the reflected spherical wave in the paraxial approximation. The angle θ plays an important role later in the computation process to eliminate the twin image and the bias term.

A point source located at the point (x_s, y_s, z_s) a distance z_s from a spherical positive lens, with focal length, induces on the lens plane a diverging spherical wave of the form of $Q(1/z_s)$. Right after the lens, which has a transmission function of $Q(-1/f)$, the complex amplitude is of a wave of the form $C_1(\bar{r}_s)Q(1/f_e)L(-\bar{r}_s/z_s)$ where $f_e=z_s f/(f-z_s)$ and the function L stands for a the linear phase function, such that $L(\bar{s})=\exp[i2\pi\lambda^{-1}(s_x x + s_y y)]$, $\bar{r}_s=(x_s, y_s)$ and $C_1(\bar{r}_s)$ is a complex constant dependent on the source point's location. On the digital camera plane at a distance d_2 from the SLM, the intensity of the recorded hologram is,

$$\begin{aligned} I_p(x, y) &= \left| C_1(\bar{r}_s) L\left(\frac{-\bar{r}_s}{z_s}\right) Q\left(\frac{1}{z_s}\right) Q\left(\frac{-1}{f}\right) * Q\left(\frac{1}{d_1}\right) \left[1 + \exp(i\theta) Q\left(\frac{-1}{a}\right) \right] * Q\left(\frac{1}{d_2}\right) \right|^2 \\ &= \left| C_2(\bar{r}_s) L\left(\frac{-\bar{r}_s f_e}{z_s(f_e + d_1)}\right) Q\left(\frac{1}{f_e + d_1}\right) \left[1 + \exp(i\theta) Q\left(\frac{-1}{a}\right) \right] * Q\left(\frac{1}{d_2}\right) \right|^2, \end{aligned} \quad (3)$$

where the asterisk denotes 2D convolution. The result of $I_p(x, y)$, after calculating the square magnitude in Eq. (3), is the PSF for any source point located at any point (x_s, y_s, z_s) on the object space of the FINCH, as follows,

$$\begin{aligned} I_p(x, y) &= A_o \left\{ 2 + \exp\left\{ \frac{i\pi}{\lambda z_R} \left[\left(x - \frac{d_2 f_e x_s}{z_s(f_e + d_1)} \right)^2 + \left(y - \frac{d_2 f_e y_s}{z_s(f_e + d_1)} \right)^2 \right] + i\theta \right\} \right. \\ &\quad \left. + \exp\left\{ \frac{-i\pi}{\lambda z_R} \left[\left(x - \frac{d_2 f_e x_s}{z_s(f_e + d_1)} \right)^2 + \left(y - \frac{d_2 f_e y_s}{z_s(f_e + d_1)} \right)^2 \right] - i\theta \right\} \right\}, \end{aligned} \quad (4)$$

where A_o is a constant and z_R , the reconstruction distance of the object point, is given by

$$z_R = \pm \frac{(f_1 + d_2)(f_e + d_1 + d_2)}{f_1 - f_e - d_1}, \text{ where } f_1 = \frac{a(f_e + d_1)}{a - (f_e + d_1)}. \quad (5)$$

The sign ' \pm ' in Eq. (5) indicates the possibility to reconstruct from the hologram either the virtual or the real image according to which term, second or third, is chosen from Eq. (4). For the special object plane of the front focal plane of the lens where $z_s=f$ the expressions in Eqs. (4) and (5) become simpler because for that plane $f_e \rightarrow \infty$ and therefore $f_1 = -a$ and $z_R = a - d_2$. The reconstruction distance of the point image from an equivalent optical hologram is z_R , although in the present case the hologram is of course digital, and the reconstruction is done by the computer. Note that z_R is obtained specifically in the case that one of the phase masks on the SLM is constant. This choice is used in all the FINCH experiments because practically the fill factor of the SLM is less than 100%, and therefore the constant phase modulation

inherently exists in the SLM. Consequently, choosing two diffractive lenses could cause unwanted three, instead of two, waves mixing on the hologram plane, one wave due to the constant phase and another two from the two different diffractive lenses.

Eq. (4) is the expression of the transparency function of a hologram created by an object point and recorded by a FINCH system. This hologram has several unique properties. The transverse magnification M_T is expressed as $M_T = \partial x_r / \partial x_s = d_2 / f$ for an object located on the front focal plane, and $M_T = f_e d_2 / z_s (f_e + d_1)$ for any other plane.

For a general 3D object $g(x_s, y_s, z_s)$ illuminated by a narrowband incoherent illumination, the intensity of the recorded hologram is an integral of the entire PSF given by Eq. (4), over all the object intensity $g(x_s, y_s, z_s)$, as follows

$$H(x, y) \cong A_0 \left\{ C + \iiint g(x_s, y_s, z_s) \exp \left[\frac{i\pi}{\lambda z_R} \left[\left(x - \frac{d_2 f_e x_s}{z_s (f_e + d_1)} \right)^2 + \left(y - \frac{d_2 f_e y_s}{z_s (f_e + d_1)} \right)^2 \right] + i\theta \right] dx_s dy_s dz_s \right. \\ \left. + \iiint g(x_s, y_s, z_s) \exp \left[\frac{-i\pi}{\lambda z_R} \left[\left(x - \frac{d_2 f_e x_s}{z_s (f_e + d_1)} \right)^2 + \left(y - \frac{d_2 f_e y_s}{z_s (f_e + d_1)} \right)^2 \right] - i\theta \right] dx_s dy_s dz_s \right\}. \quad (6)$$

Besides a constant term C , Eq. (6) contains two terms of correlation between an object and a quadratic phase function, z_s -dependent via z_R , which means that the recorded hologram is indeed a Fresnel hologram. In order to remain with a single correlation term out of the three terms given in Eq. (6), we again follow the usual procedure of on-axis digital holography. Three holograms of the same object are recorded each of which with a different phase constant θ . The final hologram H_F is a superposition according to the following equation,

$$H_F(x, y) = H_1(x, y) [\exp(\pm i\theta_3) - \exp(\pm i\theta_2)] + H_2(x, y) [\exp(\pm i\theta_1) - \exp(\pm i\theta_3)] \\ + H_3(x, y) [\exp(\pm i\theta_2) - \exp(\pm i\theta_1)], \quad (7)$$

where $H_i(x, y)$ is the i -th recorded hologram of the form of Eq. (6) and θ_i is the phase constant of the i -th SLM's quadratic phase used during the recording process. The choice between the signs in the exponents of Eq.(7) determines which image, virtual or real, is kept in the final hologram. A 3D image $g'(x, y, z)$ can be reconstructed from $H_F(x, y)$ by calculating the Fresnel propagation formula, as follows,

$$g(x, y, z) = H_F(x, y) * \exp \left[\frac{i\pi}{\lambda z} (x^2 + y^2) \right], \quad (8)$$

The system shown in Fig. 2 was used to record the three holograms (Rosen & Brooker, 2007a). The SLM (Holoeye HEO 1080P) is phase-only, and as so, the desired function given by Eq. (2) cannot be directly displayed on this SLM. To overcome this obstacle, the phase function $Q(-1/a)$ is displayed randomly on only half of the SLM pixels. These pixels were represented in the second term of Eq. (2), whereas the rest of the pixels representing the first constant term in Eq. (2) were modulated with a constant phase. The randomness in distributing the two phase functions has been required because organized non-random structure produces unnecessary diffraction orders, and therefore results in lower interference efficiency. The pixels were divided equally, half to each diffractive element, to

create two wavefronts with equal energy. By this method the SLM function becomes a good approximation to $R(x,y)$ of Eq. (2).

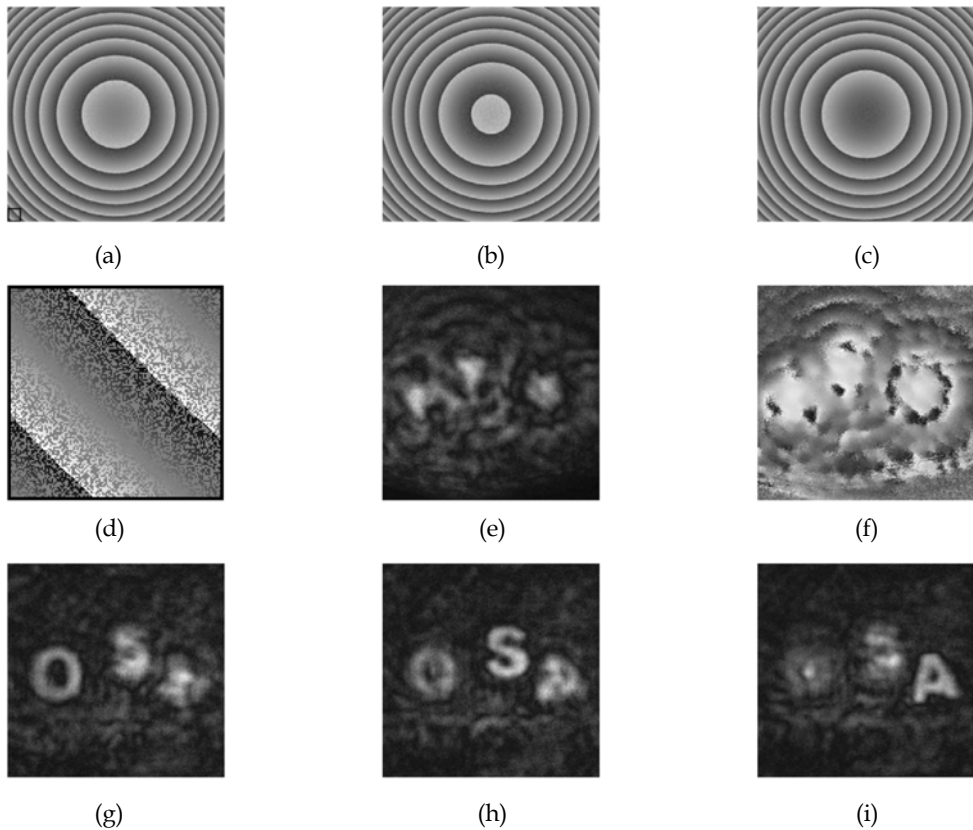


Fig. 3. (a) Phase distribution of the reflection masks displayed on the SLM, with $\theta=0^\circ$, (b) $\theta=120^\circ$, (c) $\theta=240^\circ$. (d) Enlarged portion of (a) indicating that half (randomly chosen) of the SLM's pixels modulate light with a constant phase (e) Magnitude and (f) phase of the final on-axis digital hologram. (g) Reconstruction of the hologram of the three letters at the best focus distance of 'O'. (h) Same reconstruction at the best focus distance of 'S', and (i) of 'A'.

The SLM has 1920×1080 pixels in a display of 16.6×10.2 mm, where only the central 1024×1024 pixels were used for implementing the phase mask. The phase distribution of the three reflection masks displayed on the SLM, with phase constants of 0° , 120° and 240° , are shown in Figs. 3(a), (b) and (c), respectively. The other specifications of the system of Fig. 2 are: $f=250$ mm, $a=430$ mm, $d_1=132$ mm, $d_2=260$ mm.

Three white on black letters each of the size 2×2 mm were located at the vicinity of front focal point of the lens. 'O' was at $z=-24$ mm, 'S' was at $z=-48$ mm and 'A' was at $z=-72$ mm. These letters were illuminated by a mercury arc lamp. A filter which passed a Poisson-like power spectrum from 574 to 725 nm light with a peak wavelength of 599 nm and a bandwidth (full width at half maximum) of 60 nm was positioned between the beamsplitter

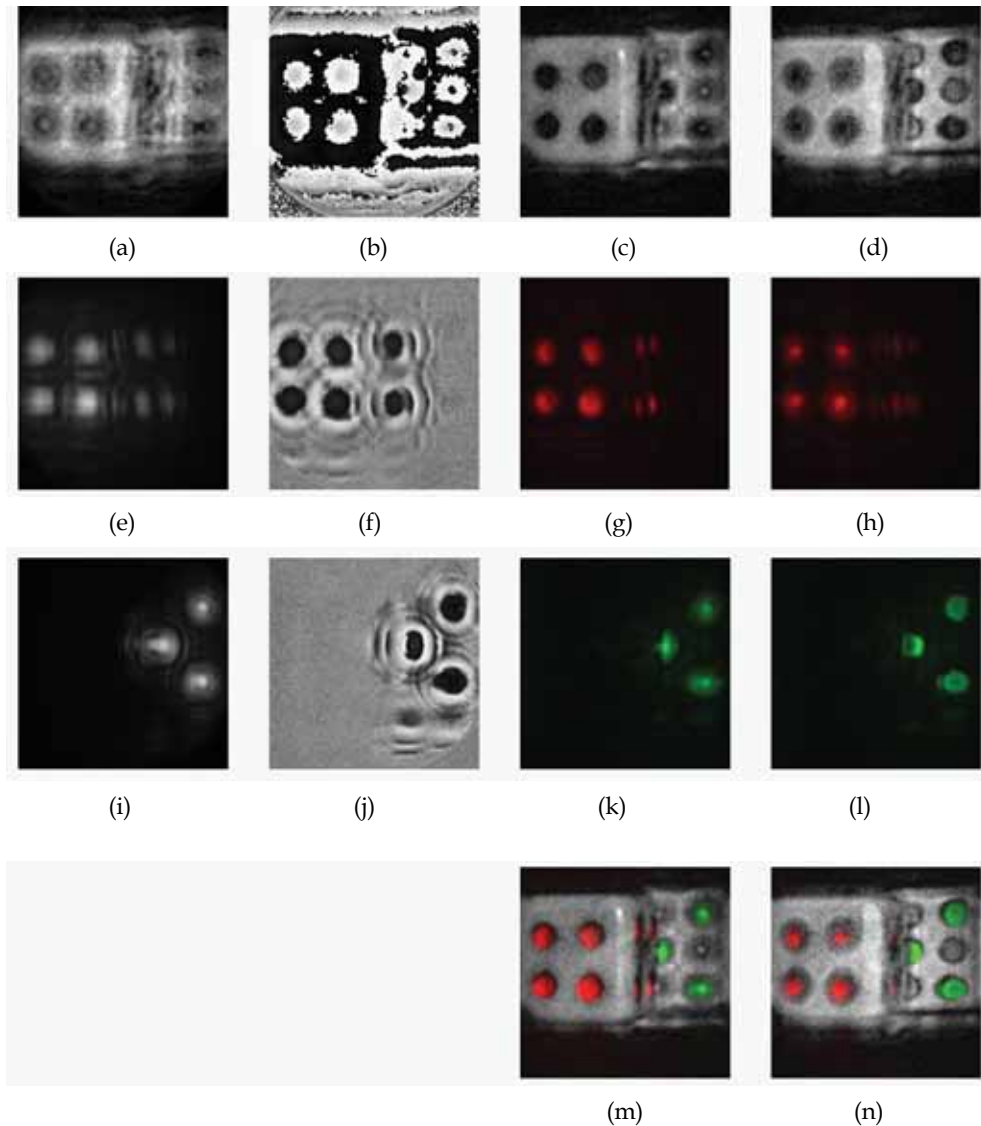


Fig. 5. (a) Magnitude and (b) phase of the complex Fresnel hologram of the dice. Digital reconstruction of the non-fluorescence hologram: (c) at the face of the red-dots on the die, and (d) at the face of the green dots on the die. (e) Magnitude and (f) phase of the complex Fresnel hologram of the red dots. Digital reconstruction of the red fluorescence hologram: (g) at the face of the red-dots on the die, and (h) at the face of the green dots on the die. (i) Magnitude and (j) phase of the complex Fresnel hologram of the green dots. Digital reconstruction of the green fluorescence hologram: (k) at the face of the red-dots on the die, and (l) at the face of the green dots on the die. Compositions of Figs 5(c), (g) and (k) and Figs 5(d), (h) and (l) are depicted in Fig. 5(m) and (n), respectively.

emission wavelength of various fluorescent dyes after excitation of 3D objects, was recorded on a digital monochrome camera after reflection from the SLM. For each wavelength of fluorescent emission, the camera sequentially records three holograms reflected from the SLM, each with a different phase factor of the SLM's function. The three holograms are again superposed in the computer to create a complex-valued Fresnel hologram of each fluorescent emission without the twin image problem. The holograms for each fluorescent color are further combined in a computer to produce a multicolored fluorescence hologram and 3D color image.

An experiment showing the recording of a color fluorescence hologram was carried out (Rosen & Brooker, 2007b) on the system shown in Fig. 4. The phase constants of $\theta_{1,2,3}=0^\circ, 120^\circ, 240^\circ$ were introduced into the three quadratic phase functions. The other specifications of the system are: $f_1=250$ mm, $f_2=150$ mm, $f_3=35$ mm, $d_1=135$ mm, $d_2=206$ mm. The magnitude and phase of the final complex hologram, superposed from the first three holograms, are shown in Figs. 5(a) and (b), respectively. The reconstruction from the final hologram was calculated using the Fresnel propagation formula of Eq. (8). The results are shown at the plane of the front face of the front die [Fig. 5(c)], and at the plane of the front face of the rear die [Fig. 5(d)]. Note that in each plane a different die face is in focus as is indeed expected from a holographic reconstruction of an object with a volume. The second set of three holograms was recorded via a red filter in the emission filter slider F_2 which passed 614 to 640 nm fluorescent light wavelengths with a peak wavelength of 626 nm and a bandwidth of 11 nm (FWHM). The magnitude and phase of the final complex hologram, superposed from the 'red' set, is shown in Figs. 5(e) and (f), respectively. The reconstruction results from this final hologram are shown in Figs. 5(g) and (h) at the same planes as shown in Figs. 5(c) and (d), respectively. Finally, an additional set of three holograms was recorded with a green filter in emission filter slider F_2 , which passed 500 to 532nm fluorescent light wavelengths with a peak wavelength of 516nm and a bandwidth of 16nm (FWHM). The magnitude and phase of the final complex hologram, superposed from the 'green' set, is shown in Figs. 5(i) and (j), respectively. The reconstruction results from this final hologram are shown in Figs. 5(k) and (l) at the same planes as shown in Fig. 5(c) and (d), respectively. Compositions of Figs. 5(c), (g) and (k) and Figs. 5(d), (h) and (l) are depicted in Figs. 5(m) and (n), respectively. Note that all the colors in Fig. 5 are pseudo-colors. These last results yield a complete color 3D holographic image of the object including the red and green fluorescence. While the optical arrangement in this demonstration has not been optimized for maximum resolution, it is important to recognize that even with this simple optical arrangement, the resolution is good enough to image the fluorescent emissions with good fidelity and to obtain good reflected light images of the dice. Furthermore, in the reflected light images in figure 5(c) and 5(m) the system has been able to detect a specular reflection of the illumination from the edge of the front die.

3.3 FINCHSCOPE – a holographic fluorescence microscope

The next system to be reviewed here is the first demonstration of a motionless microscopy system (FINCHSCOPE) based upon the FINCH, and its use in recording high-resolution 3D fluorescent images of biological specimens (Rosen & Brooker, 2008). By using high-numerical-aperture lenses, a spatial light modulator, a charge-coupled device camera and some simple filters, FINCHSCOPE enables the acquisition of 3D microscopic images without the need for scanning.

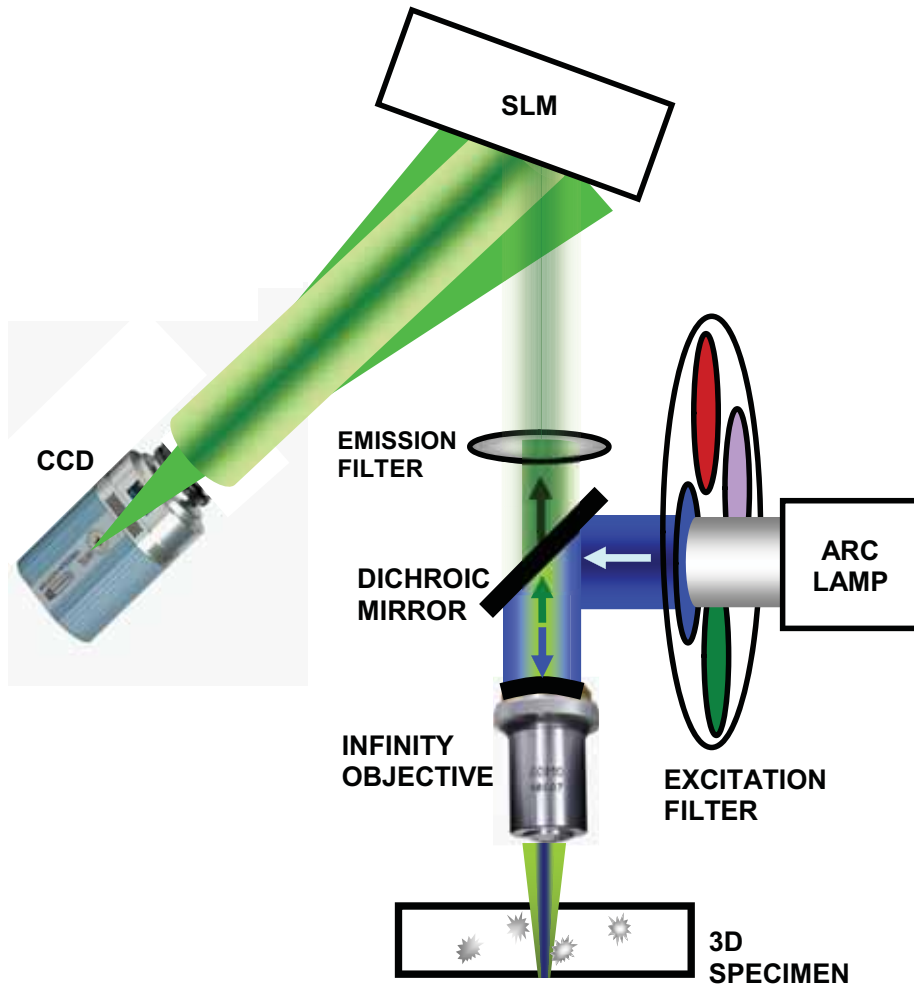


Fig. 6. FINCHSCOPE schematic in upright fluorescence microscope. The upright microscope was modified with a reflective SLM positioned at a tilt angle of 11° to reflect emission light from the objective onto the camera.

A schematic diagram of the FINCHSCOPE for an upright microscope equipped with an arc lamp source is shown in Fig. 6. The beam of light that emerges from an infinity-corrected microscope objective transforms each point of the object being viewed into a plane wave, thus satisfying the first requirement of FINCH (Rosen & Brooker, 2007a). An SLM and a digital camera replace the tube lens, reflective mirror and other transfer optics normally present in microscopes. Because no tube lens is required, infinity-corrected objectives from any manufacturer can be used. A filter wheel was used to select excitation wavelengths from a mercury arc lamp, and the dichroic mirror holder and the emission filter in the microscope were used to direct light to and from the specimen through infinity-corrected objectives.

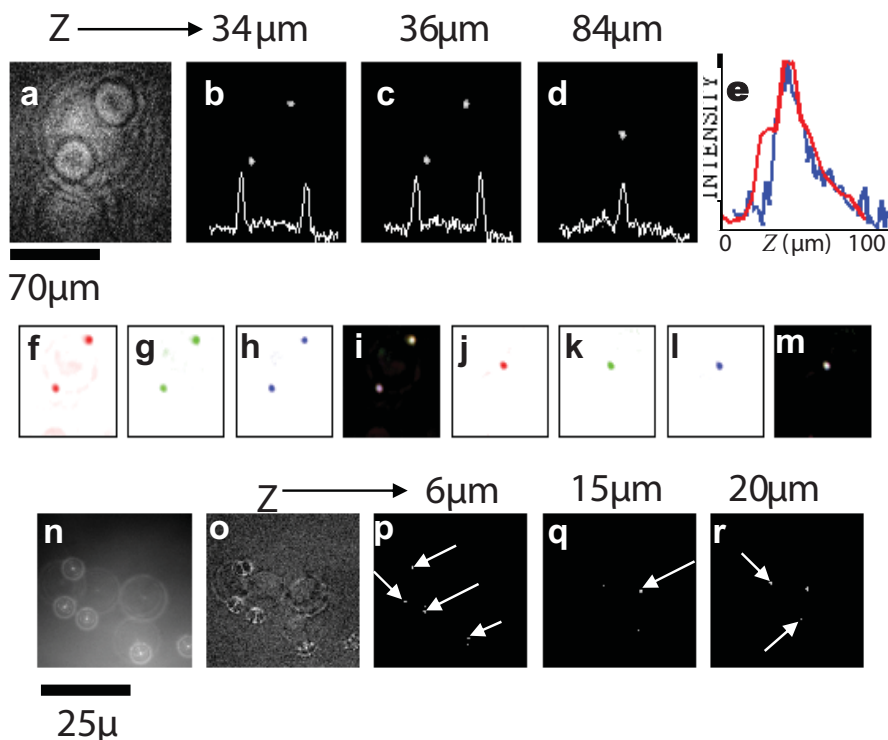


Fig. 7. FINCHSCOPE holography of polychromatic beads. (a) Magnitude of the complex hologram $6 \mu\text{m}$ beads. Images reconstructed from the hologram at z distances of (b) $34 \mu\text{m}$, (c) $36 \mu\text{m}$ and (d) $84 \mu\text{m}$. Line intensity profiles between the beads are shown at the bottom of panels b–d. (e) Line intensity profiles along the z axis for the lower bead from reconstructed sections of a single hologram (blue line) and from a widefield stack of the same bead (28 sections, red line). (f)–(h) Beads ($6 \mu\text{m}$) excited at 640, 555 and 488 nm with holograms reconstructed at planes b and (j–l) d. (i) and (m) are the combined RGB images for planes b and d, respectively. (n)–(r), Beads ($0.5 \mu\text{m}$) imaged with a 1.4-NA oil immersion objective: (n) holographic camera image; (o) magnitude of the complex hologram; (p–r), reconstructed image planes 6, 15 and $20 \mu\text{m}$. Scale bars indicate image size.

The ability of the FINCHSCOPE to resolve multicolour fluorescent samples was evaluated by first imaging polychromatic fluorescent beads. A fluorescence bead slide with the beads separated on two separate planes was constructed. FocalCheck polychromatic beads ($6 \mu\text{m}$) were used to coat one side of a glass microscope slide and a glass coverslip. These two surfaces were juxtaposed and held together at a distance from one another of $\sim 50 \mu\text{m}$ with optical cement. The beads were sequentially excited at 488, 555 and 640 nm center wavelengths (10–30 nm bandwidths) with emissions recorded at 515–535 nm, 585–615 nm and 660–720 nm, respectively. Figures 7(a)–(d) show reconstructed image planes from $6 \mu\text{m}$ beads excited at 640 nm and imaged on the FINCHSCOPE with a Zeiss PlanApo $\times 20$, 0.75 NA objective. Figure 7(a) shows the magnitude of the complex hologram, which contains all the information about the location and intensity of each bead at every plane in the field. The Fresnel reconstruction from this hologram was selected to yield 49 planes of the image, $2 \mu\text{m}$

apart. Two beads are shown in Fig. 7(b), with only the lower bead exactly in focus. The next image [Fig. 7(c)] is $2\ \mu\text{m}$ into the field in the Z -direction, and the upper bead is now in focus, with the lower bead slightly out of focus. The focal difference is confirmed by the line profile drawn between the beads, showing an inversion of intensity for these two beads between the planes. There is another bead between these two beads, but it does not appear in Figs. 7(b) or (c) (or in the intensity profile), because it is $48\ \mu\text{m}$ from the upper bead; it instead appears in Fig. 7(d) (and in the line profile), which is 24 sections away from the section in Fig. 7(c). Notice that the beads in Figs. 7(b) and (c) are no longer visible in Fig. 7(d). In the complex hologram in Fig. 7(a), the small circles encode the close beads and the larger circles encode the distant central bead. Figure 7(e) shows that the Z -resolution of the lower bead in Fig. 7(b), reconstructed from sections created from a single hologram (blue line), is at least comparable to data from a widefield stack of 28 sections (obtained by moving the microscope objective in the Z -direction) of the same field (red line). The colocalization of the fluorescence emission was confirmed at all excitation wavelengths and at extreme Z limits as shown in Figs. 7(f)–(m) for the $6\ \mu\text{m}$ beads at the planes shown in Figs. 7(b) (f–i) and 7(d) (j–m). In Figs. 7(n)–(r), $0.5\ \mu\text{m}$ beads (TetraSpeck, Invitrogen) imaged with a Zeiss PlanApo $\times 63$ 1.4 NA oil-immersion objective are shown. Figure 7(n) presents one of the holograms captured by the camera and Fig. 7(o) shows the magnitude of the complex hologram. Figures 7(p)–(r) show different planes (6, 15 and $20\ \mu\text{m}$, respectively) in the bead specimen after reconstruction from the complex hologram of image slices in $0.5\ \mu\text{m}$ steps. Arrows show the different beads visualized in different Z image planes.

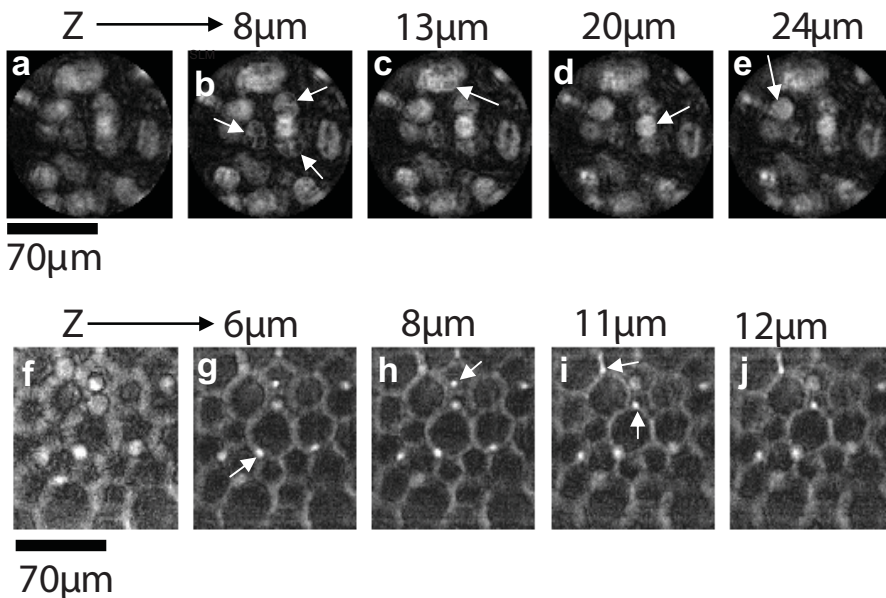


Fig. 8. FINCHSCOPE fluorescence sections of pollen grains and *Convallaria rhizome*. The arrows point to the structures in the images that are in focus at various image planes. (b)–(e), Sections reconstructed from a hologram of mixed pollen grains. (g)–(j), Sections reconstructed from a hologram of *Convallaria rhizome*. (a),(f), Magnitude of the complex holograms from which the respective image planes were reconstructed. Scale bars indicate image sizes.

The computer reconstruction along the Z-axis of a group of fluorescently labeled pollen grains (Carolina Biological slide no. 30-4264) is shown in Figs. 8(b)–(e). As is expected from a holographic reconstruction of a 3D object with volume, any number of planes can be reconstructed. In this example, a different pollen grain was in focus in each transverse plane reconstructed from the complex hologram whose magnitude is shown in Fig. 8(a). In Figs. 8(b)–(e), the values of Z are 8, 13, 20 and 24 μm , respectively. A similar experiment was performed with the autofluorescent *Convallaria* rhizome and the results are shown in Figs. 8(g)–(j) at planes 6, 8, 11 and 12 μm .

3.4 SAFE- Synthetic aperture with Fresnel elements

The recent development in FINCH is a new lensless incoherent holographic system operating in a synthetic aperture mode (Katz & Rosen, 2010). Synthetic aperture is a well-known super-resolution technique which extends the resolution capabilities of an imaging system beyond the theoretical Rayleigh limit dictated by the system's actual aperture. Using this technique, several patterns acquired by an aperture-limited system, from various locations, are tiled together to one large pattern which could be captured only by a virtual system equipped with a much wider synthetic aperture.

The use of optical holography for synthetic aperture is usually restricted to coherent imaging (Beck, et al., 2005; Mico, et al. 2006; Martínez-León & Javidi, 2008). Therefore, the use of this technique is limited only to those applications in which the observed targets can be illuminated by a laser. Synthetic aperture carried out by a combination of several off-axis incoherent holograms in scanning holographic microscopy has been demonstrated by (Indebetouw et al., 2007). However, this method is limited to microscopy only, and although it is a technique of recording incoherent holograms, a specimen should also be illuminated by an interference pattern between two laser beams.

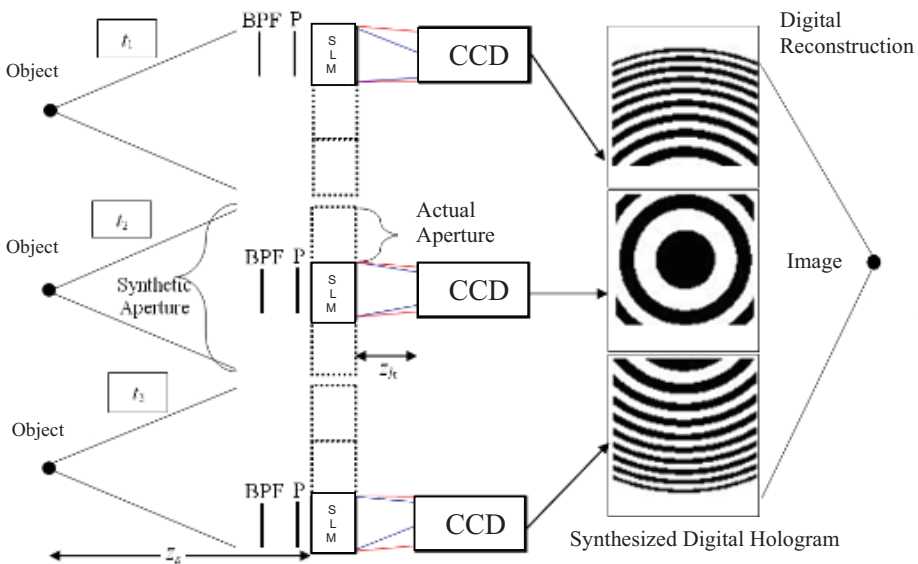


Fig. 9. Scheme of SAFE operating as synthetic aperture radar to achieve super-resolution. P indicates polarizer and BPF stands for band-pass filter.

Our new scheme of holographic imaging of incoherently illuminated objects is dubbed a synthetic aperture with Fresnel elements (SAFE). This holographic lensless system contains a band-pass filter (BPF), a polarizer, an SLM and a digital camera. SAFE has an extended synthetic aperture in order to improve the transverse and axial resolutions beyond the classic limitations. The term synthetic aperture, in the present context, means time (or space) multiplexing of several Fresnel holographic elements captured from various viewpoints by a system with a limited real aperture. The synthetic aperture is implemented by shifting the BPF-polarizer-SLM-camera set, located across the field of view, between several viewpoints. At each viewpoint a different mask is displayed on the SLM, and a single element of the Fresnel hologram is recorded (See Fig. 9). The various elements, each of which is recorded by the real aperture system during the capturing time, are tiled together so that the final mosaic hologram is effectively considered as captured from a single synthetic aperture which is much wider than the actual aperture.

An example of such system with the synthetic aperture, which is three times wider than the actual aperture, can be seen in Fig. 9. For simplicity of the demonstration, the synthetic aperture was implemented only along the horizontal axis. In principle this concept can be generalized for both axes and for any ratio of synthetic to actual apertures. Imaging with the synthetic aperture is necessary for cases where the angular spectrum of the light emitted from the observed object is wider than the numerical aperture of a given imaging system. In SAFE shown in Fig. 9, the BPF-polarizer-SLM-camera set moves in front of the object. The complete Fresnel hologram of the object, located at some distance from the SLM, is a mosaic of three holographic elements, each of which is recorded from a different position by the system with the real aperture of the size $A_x \times A_y$. The complete hologram tiled from the three holographic Fresnel elements has the synthetic aperture of the size $3 \cdot A_x \times A_y$ which is three times larger than the real aperture at the horizontal axis.

The method to eliminate the twin image and the bias term is the same as has been used before; three elemental holograms of the same object and for each point of view are recorded, each of the holograms has a different phase constant of the SLM's phase mask. The final holographic element is a specific superposition of the three recorded elements. The digital reconstruction of the final complex-valued mosaic hologram is conventionally computed by Fresnel back propagation.

SAFE has been tested in the lab by the system shown in Fig. 9. The object in this experiment is a binary grating with cycle length of 4 lines per *mm*. The distance from the object to the SLM has been 52 *cm*, and the distance between the phase-only SLM (Holoeye, PLUTO) and the digital camera (E-VISION, EVC6600SAM-GE5) has been 38.5 *cm*. A 100W Halogen ARC lamp has been used for objects illumination, and a BPF (with an 80 nm bandwidth surrounding 550 nm central wavelength) has been placed just in front of the SLM. The results of the experiments are summarized in Fig. 10. In the first experiment we have recorded a hologram only by the actual aperture without shifting the system, in the setup shown in Fig. 9 at the time t_2 . Fig. 10(a) shows one of the three masks displayed on the SLM in this experiment. Each of the three masks has one of the three different phase factors: 0° , 120° or 240° . As mentioned above, these three phase masks with different phase constants are required in order to eliminate the bias term and the twin image from the holographic reconstruction. As stated earlier, another problem with the SLM is that its fill factor is 87%, which means that part of the light is reflected from the SLM without any modulation.

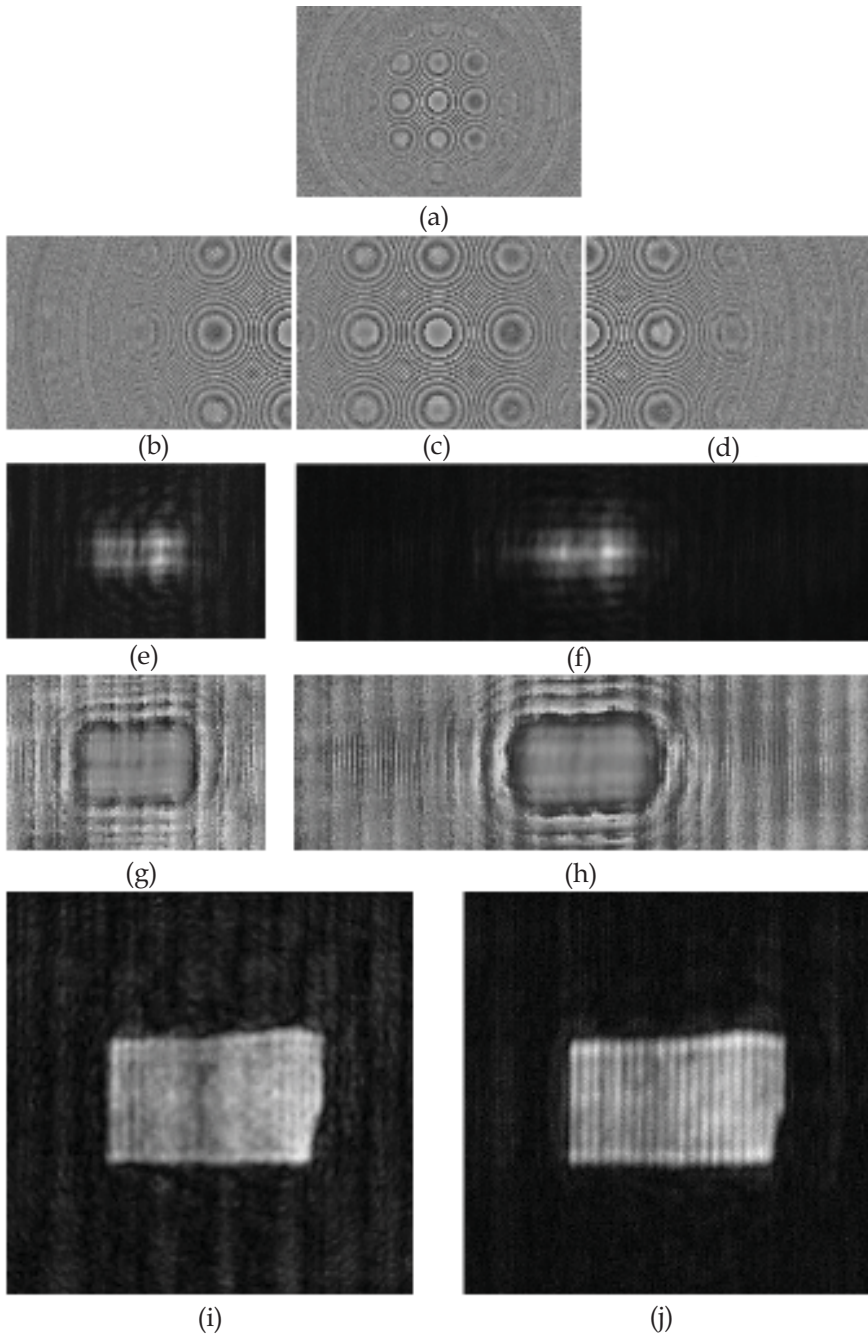


Fig. 10. Results of SAFE for the grating object with the real aperture and the synthetic aperture. See text for details.

In order to avoid the interference of three waves projected on the camera, we have chosen one of the phase elements to be constant. The other phase element has been chosen to be a negative diffractive lens with the shortest focal distance that can be achieved with the SLM having the pixel size of $8 \mu\text{m}$. The shortest focal distance guarantees maximum resolution power for a given aperture size. In the case of the actual aperture (1500×1000 pixels) and the synthetic aperture (3000×1000 pixels), the focal distances have been -34 cm and -68 cm , respectively. The input numerical aperture is 0.0115 and 0.0231 for the real and synthetic apertures, respectively, whereas the output numerical aperture is 0.0035 and 0.0044 for the real and synthetic apertures, respectively. Note that the sum of two pure phase functions, i.e., the quadratic phase function $Q[-1/a]$ and the constant phase function in Eq. (2), is no longer a pure phase function, but a complex function with non-constant magnitude. Since the SLM is a phase-only modulator, we use the previous method of recording general complex function on a phase-only SLM. Each phase function is distributed randomly among half of the SLM pixels.

The three recorded holograms are superposed according to the same superposition equation (7). Figs. 10(e), 10(g) are the magnitude and the phase of the superposed holograms for the object. It can be seen that the resolution along the horizontal direction of the reconstructed image, computed by Fresnel back propagation, is damaged in the sense that the image is lacking the original high-frequency gratings along the horizontal direction because the aperture is too narrow to capture the entire gratings spectral content. This damaged reconstructed image is shown in Fig. 10(i).

In the SAFE experiment nine different phase masks have been displayed on the SLM, three for each location of the SLM-camera set; left, central and right. Each of the masks has an actual aperture of 1500×1000 pixels. Each of the three masks at every location has one of the three different phase factors: 0° , 120° or 240° . In order to avoid edge effects on the recorded holograms there is an overlap of 750 pixels among the three actual apertures combining the synthetic aperture. For each location of the system, the three recorded holograms have been superposed as mentioned above. Figs. 10(b)-10(d) represent three masks out of nine, each of which has been displayed at different time and at a different location of the setup along the horizontal axis. The superposed complex-valued holographic element from each system's viewpoint is stored in the computer. Upon completing the system movement along the entire synthetic aperture, all three holographic elements are tiled to a single mosaic hologram. Figs. 10(f) and 10(h) represent the magnitude and the phase of the complete mosaic hologram. The reconstruction result of the mosaic hologram, computed by Fresnel back propagation, is depicted in Fig. 10(j). The binary grating on the observed objects is seen well in the reconstructed images, indicating that the synthetic aperture is wide enough to acquire most of the horizontal spectral information of the objects.

5. Discussion and conclusions

We have reviewed a new method of generating incoherent digital Fresnel holograms. The reviewed hologram, the FINCH, is actually recorded by an on-axis, single-channel, incoherent interferometer. This method inherently does not scan the object neither in the space nor in the time. Therefore, the FINCH can generate the holograms rapidly without sacrificing the system resolution. This system offers the feature of observing a complete volume from a hologram, potentially enabling objects moving quickly in three dimensions to be tracked. The FINCH technique shows great promise in rapidly recording 3D information in any scene, independently of the illumination. In addition, we have described

a rapid, non-scanning holographic fluorescence microscope that produces in-focus images at each plane in the specimen from holograms captured on a digital camera. This motionless 3D microscopy technique does not require complicated alignment or a laser. The fluorescence emission can be of relatively wide bandwidth because the optical path difference between the beams is minimal in this single-path device. Although at present each reconstructed section is not completely confocal, 3D reconstructions free of blur could be created by deconvolution of the holographic sections as is typically carried out in widefield microscopy. Time resolution is currently reduced because three holograms need to be captured sequentially. However, in the future, it will be possible to record the three holograms faster using more sensitive cameras, simultaneously capture all three holograms, or to overcome the holographic twin image problem and capture only one hologram, as any of the three holograms contain all the essential 3D information. In the present studies the image sections were obtained by a process of first capturing three holograms, computing the image z sections from the complex hologram and then, in some cases, further enhancing them by deconvolution. This process could be simplified in the future for real-time display of the holographic image, either with a holographic display system or by algorithms that create the enhanced sections and the 3D representation directly from the single hologram. There is no need for sectioning or scanning or any mechanical movement. Therefore, this system would be expected ultimately to be faster, simpler and more versatile than existing 3D microscopy techniques, which rely on pinhole imaging or deconvolution of stacks of widefield images. At present, the FINCHSCOPE is already considerably faster than conventional 3D sectioning. For example, the total image capture time for the three FINCHSCOPE images of the pollen grains in Fig. 8 was just over 1 s, compared with the 30–45 s needed to create a stack of 48 widefield or spinning disk confocal images. We have also demonstrated fluorescence holography using the high-NA objectives widely used in biological imaging. FINCHSCOPE is able to spatially resolve small beads, biological specimens and different fluorescence emission colours in x, y and z planes with perfect registration. The system provides a simple, flexible, cost-effective and powerful microscopic platform for 3D imaging.

Finally, we have demonstrated a process of recording incoherent holograms in the synthetic aperture mode. The synthetic aperture of SAFE considerably increases both the transverse and the axial resolving power. The concept of the present system can be applied to all regimes of imaging from microscopy to telescopes, and either for 2D or 3D imaging. Our demonstration of this advance in imaging, based on a new, but simple holographic principle, should open up opportunities in many life science and engineering fields, so that interesting scenes may be readily observed in three dimensions and possibly at higher resolution than with currently existing techniques.

6. References

- Beck, S. M.; Buck, J. R.; Buell, W. F.; Dickinson, R. P.; Kozlowski, D. A.; Marechal, N. J. & Wright, T. J. (2005). Synthetic-aperture imaging laser radar: laboratory demonstration and signal processing. *Applied Optics* 44(35), 7621–7629
- Breckinridge, J. B. (1974). Two-Dimensional White Light Coherence Interferometer. *Applied Optics* 13(12), 2760–2762
- Cochran, G. (1966). New method of making Fresnel transforms with incoherent light. *J. Optical Society of America* 56(11), 1513–1517
- Goodman, J. W. (1996). *Introduction to Fourier Optics*; 2nd ed. McGraw-Hill: New York, NY.

- Indebetouw, G.; Tada, Y.; Rosen, J. & Brooker, G. (2007). Scanning holographic microscopy with resolution exceeding the Rayleigh limit of the objective by superposition of off-axis holograms. *Applied Optics* 46(6), 993-1000
- Katz, B. & Rosen, J. (2010). Super-resolution in incoherent optical imaging using synthetic aperture with Fresnel elements. *Optics Express* 18(2), 962-972
- Li, Y.; Abookasis, D. & Rosen, J. (2001). Computer-generated holograms of three-dimensional realistic objects recorded without wave interference. *Applied Optics* 40(17), 2864-2870
- Lohmann, A. W. (1965). Wavefront reconstruction for incoherent objects. *J. Optical Society of America* 55(11), 1555-1556.
- Marathay, A. S. (1987). Noncoherent-object hologram: its reconstruction and optical processing. *J. Optical Society of America A* 4(10), 1861-1868
- Martínez-León, L. & Javidi, B. (2008). Synthetic aperture single-exposure on-axis digital holography. *Optics Express* 16(1), 161-169
- Mico, V.; Zalevsky, Z.; García-Martínez, P. & García, J. (2006) Synthetic aperture super-resolution with multiple off-axis holograms. *J. Optical Society of America A* 23(12), 3162-3170
- Mugnier, L. M.; Sirat, G. Y. & Charlot, D. (1993). Conoscopic holography: two-dimensional numerical reconstructions. *Optics Letters* 18(1), 66-68
- Park, J.-H.; Kim, M.-S.; Baasantseren, G. & Kim, N. (2009). Fresnel and Fourier hologram generation using orthographic projection images. *Optics Express* 17(8), 6320-6334
- Peters, P. (1966). Incoherent holograms with a mercury light source. *Applied Physics Letters* 8(8), 209-210
- Poon, T.-C. & Korpel, A. (1979). Optical transfer function of an acousto-optic heterodyning image processor. *Optics Letters* 4(10), 317-319
- Poon, T.-C. (2004). Recent Progress in Optical Scanning Holography. *J. Holography Speckle* 1(1), 6-25
- Poon, T.-C. (2007). *Optical Scanning Holography with MATLAB*. Springer, New York
- Rosen, J.; Indebetouw, G. & Brooker, G. (2006). Homodyne scanning holography. *Opt Express*, 14(10), 4280-4285.
- Rosen, J. & Brooker, G. (2007a). Digital spatially incoherent Fresnel holography. *Optics Letters* 32(8), 912-914
- Rosen, J. & Brooker, G. (2007b). Fluorescence incoherent color holography. *Optics Express* 15(5), 2244-2250
- Rosen, J. & Brooker, G. (2008). Non-Scanning Motionless Fluorescence Three-Dimensional Holographic Microscopy. *Nature Photonics* 2, 190-195
- Sando, Y.; Itoh, M. & Yatagai, T. (2003). Holographic three-dimensional display synthesized from three-dimensional Fourier spectra of real-existing objects. *Optics Letters* 28(24), 2518-2520
- Schilling, B. W.; Poon, T.-C.; Indebetouw, G.; Storrie, B.; Shinoda, K.; Suzuki, Y. & Wu, M. H. (1997). Three-dimensional holographic fluorescence microscopy. *Optics Letters* 22(19), 1506-1508
- Shaked, N. T. & Rosen, J. (2008). Multiple-viewpoint projection holograms synthesized by spatially incoherent correlation with broadband functions. *J. Optical Society of America A* 25(8), 2129-2138
- Stroke, G. W. & Restrick, R. C. III, (1965). Holography with spatially noncoherent light. *Applied Physics Letters* 7(9), 229-231
- Worthington, Jr. H. R. (1966). Production of holograms with incoherent illumination. *J. Optical Society of America* 56(10), 1397-1398